

## **New extended eddy dissipation concept model for flameless combustion in furnaces**

N. Romero-Anton<sup>a</sup>, X. Huang<sup>b</sup>, H. Bao<sup>c</sup>, K. Martin-Eskudero<sup>a</sup>, E. Salazar-Herran<sup>a</sup>, D.J.E.M. Roekaerts<sup>bc</sup>

<sup>a</sup>*ENEDI Research Group, Department of Thermal Engineering, University of the Basque Country UPV/EHU, Plaza  
Torres Quevedo 1, 48013, Bilbao, Spain*

<sup>b</sup>*Department of Process and Energy, Delft University of Technology, Leeghwaterstraat 39, Delft, CB 2628, Netherlands*

<sup>c</sup>*Department of Mechanical Engineering, Eindhoven University of Technology, P.O Box 513, Eindhoven, MB 5600,  
Netherlands*

*E-mail address: naiara.romero@ehu.eus*

### **Abstract**

Flameless combustion, also called MILD combustion (Moderate or Intense Low Oxygen Dilution), is a technology that reduces NO<sub>x</sub> emissions and improves combustion efficiency. Appropriate turbulence-chemistry interaction models are needed to address this combustion regime via computational modelling. Following a similar analysis to that used in the Extended EDC model (E-EDC), the purpose of the present work is to develop and test a Novel Extended Eddy Dissipation Concept model (NE-EDC) to be better able to predict flameless combustion. In the E-EDC and NE-EDC models, in order to consider the influence of the dilution on the reaction rate and temperature, the coefficients are considered to be space dependent as a function of the local Reynolds and Damköhler numbers. A comparative study of four models is carried out: the E-EDC and NE-EDC models, the EDC model with specific, fixed values of the model coefficients optimized for the current application, and the Flamelet Generated Manifold (FGM) model with pure fuel and air as boundary conditions for flamelet generation. The models are validated using experimental data of the Delft Lab Scale furnace (9kW) burning Natural Gas (T=446 K) and preheated air (T=886 K) injected via separate jets, at an overall equivalence ratio of 0.8. Among the considered models, the NE-EDC results show the best agreement with experimental data, with a slight improvement over the E-EDC model and a significant improvement over the EDC model with tuned constant coefficients and the FGM model.

**Key words:** Flameless combustion, MILD combustion, lab-scale furnace, Flamelet Generation Manifold, Eddy Dissipation Concept, CFD simulations.

## Nomenclature

$C_{D1}$	[-]	model parameter in EDC model
$C_{D2}$	[-]	model parameter in EDC model
$C_{\xi}$	[-]	finite structure constant in EDC model
$C_{\tau}$	[-]	residence time constant in EDC model
$c$	[-]	scaled progress variable
$\widetilde{c^2}$	[-]	scaled progress variable fluctuation
$D_a$	[-]	Damköhler number
$D_{th}$	[m <sup>2</sup> /s]	laminar thermal diffusivity
$D_{th,t}$	[m <sup>2</sup> /s]	turbulent thermal diffusivity
$\widetilde{H}$	[J/kg]	mean specific enthalpy
$k$	[m <sup>2</sup> /s <sup>2</sup> ]	turbulent kinetic energy
$L^*$	[m]	fine structure length scale in EDC model
$R_{i,r}$	[kg/(s·m <sup>3</sup> )]	net rate of production of species due to reaction r
$Re$	[-]	Reynolds number
$Re_T$	[-]	turbulent Reynolds number
$S_T$	[m/s]	turbulent flame speed (burning velocity)
$S_L$	[m/s]	laminar flame speed (burning velocity)
$T$	[K]	temperature
$u^*$	[m/s]	fine structure velocity in EDC model
$\widetilde{U}_Z$	[m/s]	mean axial velocity
$\dot{V}_a$	[nl/min]	air flow rate
$\dot{V}_f$	[nl/min]	fuel flow rate
$Y_k$	[-]	mass fraction of species k
$Y_k^{eq}$	[-]	$k^{th}$ species mass fraction at chemical equilibrium
$Y_k^u$	[-]	$k^{th}$ species mass fraction in unburnt reactant
$Y_i$	[-]	mean mass fraction in computational cell
$Y_i^*$	[-]	species mass fraction in EDC fine structure
$Z$	[-]	mixture fraction
$\widetilde{Z^2}$	[-]	mixture fraction variance

## Greek symbols

$\alpha_k$	[-]	constants in progress variable definition
$\varepsilon$	[J/(kg·s)]	turbulent energy dissipation rate
$\eta_k$	[m]	Kolmogorov length scale
$\nu$	[m <sup>2</sup> /s]	laminar kinematic viscosity
$\nu_t$	[m <sup>2</sup> /s]	turbulent kinematic viscosity
$\xi^*$	[-]	(normalized) fine structure length in EDC model
$\rho$	[kg/m <sup>3</sup> ]	mean density

$\tau_c$	[s]	chemical time scale
$\tau_k$	[s]	Kolmogorov time scale
$\tau_c^*$	[s]	chemical time scale of fine structure in EDC model
$\tau^*$	[s]	residence time scale in EDC model
$\Phi$	[-]	equivalence ratio

#### *Abbreviations*

CARS	Coherent Anti-stokes Raman Spectroscopy
CFD	Computational fluid Dynamics
DNS	Direct Numerical Simulations
DO	Discrete Ordinate
EDB	Eddy Break Up model
EDC	Eddy Dissipation Concept model
EDM	Eddy Dissipation model
E-EDC	Extended Eddy Dissipation Concept
FGM	Flamelet Generated Manifold
FPV	Flamelet Progress Variable
GCI	Grid Convergence Index
HR	Formylradical
JHC	Jet-in-Hot-Coflow
LDA	Laser Doppler Anemometry
MILD	Moderate or Intense Low Oxygen Dilution
NE-EDC	Novel Extended Eddy Dissipation Concept
PaSR	Partially Stirred Reactor
PDF	Probability Density Function
PFR	Plug Flow Reactor
PSR	Perfectly Stirred Reactor
RANS	Reynolds-Averaged Navier–Stokes
RSM	Reynolds-stress-model
WSGGM	Weighted-Sum-of-Grey-Gases Model

## 1 Introduction

The main goals of industrial furnace design are to achieve a controlled, in general homogeneous, temperature distribution in every furnace zone, with efficient energy use and savings, as well as low pollutant emissions. Flameless combustion is a key technology towards obtaining these goals [1]-[2] based on the dilution of fuel and air stream by the aerodynamic recirculation of the flue gas. Mixing with recirculated products is responsible for the main characteristics: namely, diluted reaction zones, uniform temperature distribution, non-visible or audible flames, and low thermal  $\text{NO}_x$  emissions. It is applied in industrial boilers and furnaces, as well as being explored for application in gas turbines [3].

A better understanding of flameless combustion is needed in order to establish the methodology of furnace design to reduce fuel consumption and pollutant emissions. To this end, lab-scale and semi-industrial scale experiments and Computational Fluid Dynamics (CFD) simulations have been carried out [4].

The experimental configurations studying flameless combustion can be divided into two classes: unconfined and confined. In the first, most of the experiments concern Jet-in-Hot-Coflow (JHC) burners, mimicking the mixing by recirculated products via a controlled mixing in a secondary burner [5]-[8]. The second includes a number of lab-scale furnaces with a single burner [9]-[13] and a few with more burners, approaching industrial and semi-industrial furnaces [14]-[16]. The data from these experiments have been used to gain insights into the combustion process and to validate simulation results.

Perpignan et al. [4] also reviewed the modelling approaches developed for the numerical simulation of flameless combustion. The EDC model has been applied extensively since the start of the research into this area. Cabra et al. [6] compared transported PDF with standard EDC using both the standard  $k - \epsilon$  turbulence model and the Reynolds-stress-model (RSM). Tabacco et al. [17] investigated flameless combustion using the standard EDC and PDF. Christo and Dally [18] studied the Adelaide JHC burner by numerical simulation, comparing the EDC, EDM, Flamelet-based and PDF models. In these works, however, the simulation results did not match well with experimental data, showing that combustion models developed for conventional combustion often do not accurately describe the consequence of the dilution by recirculated products, resulting in the over prediction of the temperature of the combustion gases (at least locally). This occurs in the EDC model because the EDC values were empirically chosen for conventional combustion, while in flameless combustion, due to the dilution, the temperature of the furnace is reduced and, consequently, chemical time scales (reaction region) increase. These specific flameless combustion features are not considered in the standard EDC model, so its constant modification has been proposed [19]-[22]. As a first approach, the finite structure constant  $C_\xi$  and the residence time constant  $C_\tau$  (explained in section 2.2) were changed, calibrating them with experimental data. Lewandowski and Ertesvåg [23] and Ertesvåg [24] made a complete, systematic review of these approaches, introducing modified values of the model parameters.

The review by Ertesvåg [24] also benchmarks the proposed modifications with respect to the original principles and the consistency conditions of the EDC model formulation proposed in the works by Magnussen and co-workers [25]-[26]. In order to reduce the dependency on experimental data and also make the EDC more widely applicable to flameless combustion systems, Parente et al. [27] took an important step by proposing an extension to the EDC model (here called E-EDC), where model constants depend on the local Reynolds and local Damköhler numbers.

The nature of the reaction zones in flameless combustion and the implications for modelling have been the subject of many studies. A substantial part of them was reviewed in Ref [4]. It is clear that turbulence-chemistry interaction models based on thin reaction zones (flamelet-based models) or models calibrated for conventional combustion conditions, such as the standard EDC models, fail to give accurate predictions. This is often attributed to the presence of distributed reaction zones. As demonstrated by Chen et al [28]-[29], simply using a perfectly stirred reactor (PSR) model can provide better results than flamelet or EDC models. The PSR model was applied in an Adelaide JHC burner [28] for an adiabatic case, as well as to a non-adiabatic cyclonic combustor furnace [29].

To provide a more fundamental understanding and possible explanations of the reasons why models have a certain performance, Minamoto et al. [30]-[33] made several DNS studies of the special characteristics of the flame front structure under flameless combustion. These studies concerned the evolution and interaction of flame fronts in initially homogeneous isotropic turbulence in a cubical volume bounded by symmetry or periodic boundaries. They used a skeletal mechanism with 16 species and 36 reactions and a non-unity Lewis number for species transport. The results revealed a complex flame structure. The PDF of the reaction progress variable, based on temperature ( $C_T$ ), presented a wide range of intermediate values between 0 and 1. This was in contrast to standard thin premixed reaction fronts, where the probability of finding intermediate values between 0 and 1 is very small. However, the PDF of the reaction progress variable, based on the fuel species mass fraction ( $C_Y$ ), provided a bimodal distribution suggesting thin reaction zones. The experimental results of Refs. [8]-[9],[34], and the Direct Numerical Simulation (DNS) results of Refs. [30]-[33], were found to be consistent with each other: OH-PLIF and  $C_Y$  suggested thin reaction zones, while temperature images and  $C_T$  showed more similar distributed reaction zones. Therefore, it may be concluded that combustion structures in this regime can be described as small flamelets interacting with each other. The DNS results also suggested that, depending on the dilution level, the interaction between the thin reaction zones varies; that is, sustained interaction between the thin reaction zones occurs at high dilution levels, while little interaction occurs at a low dilution level.

Minamoto and Swaminathan [31] investigated how good mean reaction rates in the DNS of MILD combustion are described by three 'paradigms': standard flamelets based on pure fuel and pure oxidiser, flamelets based on diluted streams ('mild flame elements'), and a PSR with the size of the laminar flame thickness. They concluded that the pure fuel and pure air flamelets are not

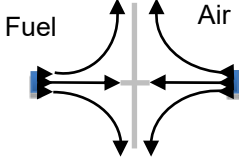
suitable, that the diluted flamelets give qualitative agreement and the PSR-based model is appropriate. Here, the well stirred reactor was assumed to be the size of a representative laminar flame thickness (thermal thickness or Zeldovich thickness). The concept of interaction between reaction zones was recently adopted in an extension of the EDC model by Evans et al. [35]. The results showed better agreement with the experimental data. The improvement also consisted in calculating the reaction time scale considering the reaction rate of several main species: CH<sub>4</sub>, CO, H<sub>2</sub>, O<sub>2</sub> and CO<sub>2</sub>.

In this work, a new model called the New Extended EDC model (NE-EDC) is developed (see section 2.3) and tested with the Delft lab-scale furnace experimental data. It is intended to be an accurate and computationally affordable turbulence-chemistry interaction model suitable for the accurate simulation of flameless combustion without the need for extensive case-by-case model calibration. To judge the performance, the predictions will be compared to those of existing EDC and flamelet-based models [19],[27],[36]-[38]. Following a similar analysis to that used in the E-EDC model developed by Parente et al. [27], in the NE-EDC model, the coefficients are calculated based on the local Reynolds number and the Kolmogorov scale Damköhler number. The E-EDC and the NE-EDC both introduced fine structures characterising chemical conversion. They differ in the postulated length scale of the structures, but agree in giving them the turbulent velocity as velocity scale. The E-EDC associates a length scale of the laminar flame thickness type with them, obtained as a product of the laminar flame speed and the chemical time scale. On the other hand, the NE-EDC associates the Kolmogorov scale with the structures and avoids the need for calibrating a proportionality factor in an expression for laminar flame speed.

This study describes the differences between the two models in detail and compares their predictions in the application to the Delft lab-scale furnace in flameless combustion mode at power 9 kW [36]-[37]. This lab-furnace has several advantages when compared to other experimental setups: (1) in contrast to the JHC burners, the setup includes both the aerodynamic recirculation of products and the important influence of radiative heat transfer; (2) in contrast to larger furnaces, it is fully accessible for non-intrusive measurements, while detailed statistics of velocity and temperature are available for model validation; (3) it does not have cooling tubes inserted as a heat sink into the furnace [39], making the flow patterns easier to compute.

To widen the basis of the validation of the NE-EDC model, this study also compares its predictions: firstly with those of the EDC with a modified but spatially homogeneous value of the EDC fine structure constant  $C_{\xi}$ , which is optimized through a parametric analysis developed in this paper; and secondly with the FGM model using non-premixed flamelets of fuel and air. Key aspects of the turbulence-chemistry interaction models compared in this work are summarised in Table 1.

*Table 1 Key aspects of the principles of the turbulence-chemistry interaction models used in this study*

<b>FGM</b> (ANSYS Fluent default options)	Pure fuel and air as boundary conditions for flamelet generation		
<b>EDC</b> (Parametric study for Delft lab-scale flameless furnace)	EDC $C_\xi$ modified		
<b>E-EDC</b> (Parente et al. [27])	$\left. \begin{aligned} C_\xi &= f_1(Re_T, Da^*) \\ C_\tau &= f_2(Re_T, Da^*) \end{aligned} \right\} \longrightarrow$	<b>NE-EDC</b> (developed)	$\left. \begin{aligned} C_\xi &= f_3(Re_T, Da^*) \\ C_\tau &= f_4(Re_T, Da^*) \end{aligned} \right\}$

The results in velocity and temperature distribution obtained from the different models are compared with the experimental data.

## 2 Turbulence combustion interaction models

In this section, the turbulent combustion models used in this work are described. First, a short summary is given of the FGM model and the EDC model with modified constant model coefficients. Then the extended EDC models are described; first the E-EDC model of Parente et al. [27]) followed by the novel extended EDC (NE-EDC) model. The differences between both extended models are explained. Finally, arguments are provided showing that, as with the original EDC, the new models effectively provide evolution in the composition space in a reduced manifold.

### 2.1 FGM model

The FGM model is based on the assumption that the local state of the reacting mixture evolves in the same way as one of a set of canonical cases of simple laminar flame structures. The relations between all relevant variables and a selected number of variables describing the local state (mixture fraction ( $Z$ ) and scaled reaction progress variable ( $c$ )) define a manifold in the composition space. In contrast to the purely chemical reduction methods, the FGM model also takes into account the role of diffusion (transport effects) and can also accurately describe states at low temperatures outside the main reaction zone. In contrast to the steady flamelet model, the selection of the local state is not primarily controlled by the strain rate, but by a chemical source term of progress variable.

The application of the FGM model requires less computational time than the EDC model, since detailed chemistry is only used in the manifold creation, whereas relevant quantities in the turbulent flow are retrieved from the lookup tables.

The scaled progress variable,  $c$  ( $Z$ ), describes the reaction progress from a value equal to 0 in the unburnt gases to 1 in the fully burnt gases. In the ANSYS Fluent implementation, the un-

normalized progress variable is calculated as the sum of the product species mass fraction relative to the species mass fraction in equilibrium and the unburnt state:

$$\tilde{c} = \frac{\sum_k \alpha_k (Y_k - Y_k^u)}{\sum_k (Y_k^{eq} - Y_k^u)} \quad (1)$$

where  $\alpha_k$  are constants that are typically zero for reactants and unity for a few product species. Here,  $\alpha_{CO_2} = \alpha_{CO} = 1$  is used and zero for the other species. To take into account heat loss, local states with heat loss are constructed by reducing the temperature at the boundary of the flamelet computational domain. The maximum enthalpy loss considered in the table generation is determined from the lowest experimentally observed mean temperature of the mixture in the furnace interior, in this case, 951 K. In the implementation of the FGM method in ANSYS Fluent, the flamelets underlying the manifold are based on fuel and air as the incoming stream. Steady non-premixed flamelets are considered and, increasing the scalar dissipation rate, in total 64 flamelets are generated until extinction is reached [40]. The generalization of FGM, consisting of including the effect of the recirculation of products during flamelet creation, as proposed by Huang [37], is not among the default options offered by ANSYS Fluent and has not been used.

In order to take into account the influence of turbulent fluctuations, it is assumed that the mixture fraction and the scaled progress variable are statistically independent and that both have a  $\beta$ -function PDF, fully characterized by the mean and the variance. Fluctuations in the enthalpy loss (relative to the adiabatic conditions) are neglected. Finally, the resulting FGM table for the mean properties (including the mean chemical source term) has five independent variables and provides relations of the form:

$$\tilde{\varphi} = \tilde{\varphi}(\tilde{Z}, \tilde{Z}^2, \tilde{c}, \tilde{c}^2, \tilde{H}) \quad (2)$$

where  $\tilde{H}$  denotes the enthalpy loss, obtained from the equation for mean enthalpy.

## 2.2 EDC with modified constant model coefficients

The original EDC model proposed by Magnussen and co-workers [41] assumes that the reactions are fast and occur in small zones that are modelled as a chemical reactor. The model conceptually divides every computational cell into two zones: the fine structures, where chemical reactions occur, and the surrounding fluid. The properties of the fine structures are denoted by a superscript ‘\*’, e.g., the length and velocity scales are denoted by  $L^*$  and  $u^*$ . They are assumed to be on the same scale as the smallest scale of turbulence, the Kolmogorov scale. Both large and small turbulence scales are taken into account to set the residence time in the small reaction zones and the mass transfer to these zones. The fine structures were originally assumed to be PSR (chemical reaction in the presence of infinitely fast mixing) [42], but in the version implemented in ANSYS Fluent [40], the fine structures are represented as a Plug Flow Reactor (PFR) (chemical evolution in time, with no mixing). Ertesvåg [24] has discussed the implications of this difference in detail. After some derivation, it is found that the reaction rate of the mean mass fraction of a species is of the form given by Eq. (3) [19]:



$$R_{i,r} = \frac{\bar{\rho}(\xi^*)^2}{\tau^*[1 - (\xi^*)^3]}(Y_i^* - Y_i) \quad (3)$$

Here,  $\xi^*$  is a fine structure length scale based on the ratio of the mass of regions containing fine structures and the total mass, while  $\tau^*$  is the fine structure residence time based on the mass transfer rate between the fine structures and the surroundings. In the PFR model, the mass fractions  $Y_i^*$  are recalculated every computational time step by integrating the chemical kinetics, starting from the current cell mean value up to a later time proportional to the Kolmogorov time scale. Depending on additional assumptions, somewhat different expressions have also been derived [25]-[26] and these have been reviewed in Refs.[43] and [24]. In Eq. (3), the turbulence-chemistry interaction is only taken into account via the estimates of the volume fraction of the fine structures and the transfer rates based on the energy cascade concept and not via fluctuations in local properties.

Using an analysis of the energy-cascade concept for the mechanical energy in the turbulent flow, it can be shown that the energy dissipation rate ( $\varepsilon$ ) is related to the properties of the fine structures via Eq. (4) and Eq. (5) [44]:

$$\varepsilon = \frac{4}{3}C_{D2}v\frac{u^{*2}}{L^{*2}} \quad (4)$$

$$\varepsilon = 2C_{D1}\frac{u^{*3}}{L^*} \quad (5)$$

The model constants were calibrated with experimental data on turbulent flows to the values  $C_{D1} = 0.135$  and  $C_{D2} = 0.5$  [40]. Defining and evaluating the Reynolds number of the fine structure by Eq. (6), it can be seen that the fine structures are indeed in the dissipative range, since the Reynolds number is of order unity:

$$Re = \frac{u^*L^*}{v} = \frac{2C_{D2}}{3C_{D1}} \approx 2.5 \quad (6)$$

In the EDC model derivation based on the energy cascade concept, the fine structure length  $\xi^*$  and the residence time scale  $\tau^*$  are given by Eq. (7) and Eq. (8).

$$\xi^* = \left(\frac{3C_{D2}}{4C_{D1}^2}\right)^{1/4} \left(\frac{v\varepsilon}{k^2}\right)^{1/4} = C_\xi \left(\frac{v\varepsilon}{k^2}\right)^{1/4} \quad (7)$$

$$\tau^* = \left(\frac{C_{D2}}{3}\right)^{1/2} \left(\frac{v}{\varepsilon}\right)^{1/2} = C_\tau \left(\frac{v}{\varepsilon}\right)^{1/2} \quad (8)$$

The relation between the model constants  $C_\xi$  and  $C_\tau$  and the model constants  $C_{D1}$  and  $C_{D2}$  is  $C_{D1} = \frac{3}{2} \frac{C_\tau}{C_\xi^2}$  and  $C_{D2} = 3C_\tau^2$ , leading to  $C_\xi = 2.1377$  and  $C_\tau = 0.4082$ .

Since the finite structure constant,  $C_\xi$ , is proportional to the EDC model fine structure length  $\xi^*$  calculation and the residence timescale,  $\tau^*$ , is the product of the residence time constant,  $C_\tau$ , and

the Kolmogorov time scale; then the impact of the value of the constants on the mean reaction rate (Eq. (3)), and consequently on the composition and temperature prediction, is very direct.

In flameless combustion, the reaction zones are thicker and the temperature gradients in the mean profile are significantly lower than in conventional combustion. It has been found that these differences lead to a bad agreement between modelling results and experimental data when the EDC model, with standard values of the model parameters  $C_\xi$  and  $C_\tau$ , is used. The literature has investigated whether changing the constant value of the model parameters can result in better predictions in flameless combustion [23]-[24].

In the present work, an optimization of the spatially constant value of the model constants for the current lab-scale furnace is made. In some of the earliest studies considering the optimization of the model constant values, Rehms [21] and Graça [45] concluded that, when selecting a different value for the model constants in flameless combustion applications, the best results are obtained by leaving the residence time constant,  $C_\tau$ , unchanged and increasing the value of the finite structure constant,  $C_\xi$ . Following this observation, in this work, the results of several simulations are presented, considering different values of  $C_\xi$ :  $C_\xi = 2.1317$  (original),  $C_\xi = 2.4$ ,  $C_\xi = 2.9$ ,  $C_\xi = 3.7$ ,  $C_\xi = 4.5$ , and  $C_\xi = 5$  (see subsection 4.1). This range of variation is within the acceptable range of variation proposed by Ertesvåg [24].

### 2.3 E-EDC and NE-EDC models

In the literature, it has been shown that the EDC model, with the standard values of the model parameters  $C_\xi = 2.1377$  and  $C_\tau = 0.4082$ , often over predicts furnace temperature. These constant values were empirically selected considering conventional combustion characteristics; therefore, they do not take into account the dilution effect present in flameless combustion. As a solution, Parente et al. [27] proposed an Extension of the EDC model (here called E-EDC) with constants  $C_\tau$  and  $C_\xi$  depending on the local Reynolds and Damköhler numbers. In the present work, following a similar analysis to that of the E-EDC model, but using an alternative set of assumptions, a modification is proposed leading to a novel extension of the EDC model (called NE-EDC).

The first assumption of Parente et al. is that, due to the high dilution in flameless combustion, the size of the reacting structures can extend over a range of turbulent length scales and is, in general, larger than the Kolmogorov length scale [46]. Therefore, the length scale of the reacting fine structures,  $L^*$ , is chosen to be different from the Kolmogorov length scale ( $\eta = (v^3/\varepsilon)^{1/4}$ ) and its value has to be determined. The velocity of the reacting fine structure  $u^*$  is assumed to be equal to the turbulent flame speed  $S_T$ , ( $u^* = S_T$ ). Since the Damköhler number is low in flameless combustion and there is high intensity turbulence, the ratio of the turbulent flame speed to the laminar flame speed is calculated from the ratio of the turbulent thermal diffusivity  $D_{th,t}$  to the laminar thermal diffusivity  $D_{th}$  using [47]:

$$S_T \approx S_L \sqrt{\frac{D_{th,t}}{D_{th}} + 1} \approx S_L \sqrt{\frac{v_t}{v} + 1} \approx S_L \sqrt{Re_T + 1} \quad (9)$$

Here, the laminar and turbulent Prandtl numbers have been assumed to be equal to unity, where  $Re_T$  is the turbulent Reynolds number and  $S_L$  is the laminar flame speed, which is estimated from [47]:

$$S_L \propto \sqrt{v/\tau_c} \quad (10)$$

Using these assumptions, it follows that the ratio of the model constants  $C_{D2}$  and  $C_{D1}$  is given by:

$$\frac{C_{D2}}{C_{D1}} = \frac{3u^*L^*}{2v} = \frac{3S_L\sqrt{Re_T+1}}{2v}L^* \propto \frac{3L^*\sqrt{Re_T+1}}{S_L\tau_c} \quad (11)$$

Assuming that the chemical reaction time scale is the time a laminar flame needs to cross another laminar flame and considering that, in the EDC model, the reacting fine structure is the flame, an estimate of the thickness of the reacting fine structure can be obtained as follows:

$$L^* = S_L\tau_c \quad (12)$$

Using Eq. (12) one obtains:

$$\frac{C_{D2}}{C_{D1}} \propto \frac{3}{2}\sqrt{Re_T+1} \quad (13)$$

Defining a Damköhler number based on the Kolmogorov time scale,  $Da^* = \tau_k/\tau_c$ , an expression where the  $C_{D2}$  constant depends on the Reynolds and Damköhler local values is obtained:

$$C_{D2} = \frac{3}{4} \frac{1}{(Re_T + 1)Da^*} \quad (14)$$

$C_{D2}$  and  $C_{D1}$  model constants are related via Eq. (11) and it follows that:

$$C_{D1} \propto C_{D2} * \frac{1}{\sqrt{Re_T+1}} \propto \frac{1}{(Re_T+1)^{3/4} Da^*} \quad (15)$$

Finally, using the relation between the model constants  $C_\xi$  and  $C_\tau$  and the model constants  $C_{D1}$  and  $C_{D2}$ , expressions for  $C_\xi$  and  $C_\tau$  depending on the Reynolds and Damköhler number values are obtained:

$$C_\tau = \left(\frac{C_{D2}}{3}\right)^{1/2} \propto \frac{1}{\sqrt{(Re_T+1)Da^*}} \quad (16)$$

$$C_\xi = \left(\frac{3C_{D2}}{4C_{D1}^2}\right)^{1/4} \propto \sqrt{(Re_T+1)Da^*} \quad (17)$$

It should be noted that, in a recent work, Evans et al. [35] have extended the approach of E-EDC, replacing the proportionality present in Eq. (16) and Eq. (17) by an equality with a constant coefficient, leading to Eq. (18) and Eq. (19):

$$C_\tau = \left(\frac{C_{D2}}{3}\right)^{1/2} = \frac{1}{2} \frac{1}{\sqrt{(Re_T + 1)Da^*}} \quad (18)$$

$$C_\xi = \left(\frac{3C_{D2}}{4C_{D1}^2}\right)^{1/4} = \left(\frac{2}{3}\right)^{1/2} \sqrt{(Re_T + 1)Da^*} \quad (19)$$

This extension has not been included in the validation study presented below.

The residence time constant is inversely proportional to  $Da^*$ , whereas the fine structure constant is proportional to  $\sqrt{Da^*}$ . The value of the turbulent Reynolds number is obtained from the properties provided by the turbulence model. The determination of the  $Da^*$  value also needs an estimation of the chemical time scale from the chemical mechanism and local conditions. Parente et al. [27] used the new expressions for the model constants in two ways. A first approach is to use simulation results to estimate the best global values of  $Re_T$  and  $Da^*$  and use these to identify the best global values of the model constants. A second approach is to evaluate  $Re_T$  and  $Da^*$  from local states and use locally varying values of  $C_\xi$  and  $C_\tau$ .

The chemical time scale was obtained from a one-step reaction, using the temperature and main species concentrations coming from the detailed mechanism used for the gas phase reactions. Both approaches and the EDC with standard values of the model constants were applied to several cases of the Adelaide jet-in-hot-coflow experiments. It was found that the modification of the EDC model coefficients improves the predictions close to the burner, whereas re-ignition phenomena farther away have not yet been reproduced. The latter was attributed to limitations of the Reynolds-Averaged-Navier-Stokes (RANS) approach rather than the EDC model. In the application considered here, the fuel and air jets are confined by the furnace walls and surrounded by products, while the downstream re-ignition present in the JHC configuration are absent. While preparing for the application of the E-EDC model to the application of the lab scale furnace, the assumptions of the model were reviewed and an alternative formulation (here called NE-EDC) has been developed as described below.

First, unlike in the E-EDC model developed by Parente et al. [27], in the new model proposed here, the length scale of the reacting fine structure is assumed to be the Kolmogorov length scale ( $L^* = \eta_k$ ). This is consistent with the derivation of the EDC reaction rate derived from an energy cascade concept with an energy cascade extending to the Kolmogorov scale. Nevertheless, it is proposed here as a method to handle the fact that, according to the DNS results and the experimental  $OH^*$ -luminescence observations by Huang [37], there is no collection of well-defined isolated reaction zones in flameless combustion. Instead, a conglomerate of several flame fragments touching each other are present. This makes it hard to choose the size to define the fine structure of the system. Therefore, instead of basing the fine structure size on flame thickness, in this work, the size is chosen based on the velocity field. A region smaller than the

Kolmogorov scale is homogeneous in velocity and, in all cases where chemical fronts are thicker than the Kolmogorov scale, a structure of that scale can be considered to be homogeneous and not disturbed by the flow field. This leaves the possibility open that significant variation in composition is only seen over a significantly larger scale than the Kolmogorov scale.

Secondly, the use of the expression for the laminar flame speed containing a proportionality factor (Eq. (10)) is avoided by eliminating the laminar flame speed from the equations. Thus, a quantitative prediction for the model constant values is obtained without the proportionality factor. In the NE-EDC model, as in the E-EDC, it is assumed that the fine structure velocity scale ( $u^*$ ) is the characteristic speed of the turbulent mixture of multiple reacting fine structures ( $u^* = S_T$ ). Here, the turbulent flame speed is used because it is an overall measure of the conversion in a complex reacting flow. In flameless combustion, the reacting mixture consists of a conglomerate of local structures. Experimental data [48] indeed show that ignition kernels are continuously forming and growing in size. Multiple developing and combining kernels represent the overall combustion. The conversion of reactants in the mix of local structures is characterised by the turbulent burning velocity ( $S_T$ ). This velocity is identified with the fine structure velocity ( $u^*$ ) and is different from the Kolmogorov scale velocity. The NE-EDC model uses the same Damköhler expression for the ratio between the turbulent and laminar flame speeds:  $S_T = S_L \sqrt{Re_T + 1}$ .

Next, a fine structure chemical time scale is defined by  $\tau_c^* = L^*/S_L$ . Taking this equation into account, an alternative expression for Eq. (11) is obtained that does not contain the laminar flame speed:

$$\frac{C_{D2}}{C_{D1}} = \frac{3u^*L^*}{2v} = \frac{3S_L\sqrt{Re_T + 1}}{2v}L^* = \frac{3\sqrt{Re_T + 1}L^{*2}}{2v\tau_c^*} \quad (20)$$

As the fine structure length scale is assumed to be the Kolmogorov scale, the term  $L^{*2}/v\tau_c^*$  is equal to the Kolmogorov scale's Damköhler number

$$\frac{L^{*2}}{v\tau_c^*} = \frac{(v/\varepsilon)^{1/2}}{\tau_c^*} = \frac{\tau_k}{\tau_c^*} = Da^* \quad (21)$$

Then, the following final expressions for  $C_\xi$  and  $C_\tau$ , are obtained:

$$C_\tau = \left(\frac{C_{D2}}{3}\right)^{1/2} = \frac{1}{2} \frac{1}{\sqrt{(Re_T + 1)Da^*}} \quad (22)$$

$$C_\xi = \left(\frac{3C_{D2}}{4C_{D1}^2}\right)^{1/4} = \sqrt{\frac{3}{2}(Re_T + 1)Da^{*3/4}} \quad (23)$$

In Eq. (22) and Eq. (23), the model coefficients are calculated as functions of the local  $Re_T$  and  $Da^*$  numbers. The difference with the E-EDC model is that the finite structure constant  $C_\xi$  is found to be proportional to  $Da^{*3/4}$  and not to  $Da^{*1/2}$ . This difference arises because the definition of the chemical time scale is different. The one used in the NE-EDC is the time needed for a premixed

flame to travel a distance equal to the Kolmogorov scale, while moving with the laminar flame speed. In this study, this chemical time scale was obtained from the rate of a one-step mechanism. It has been evaluated as the inverse of an Arrhenius reaction rate as  $\tau_c^* = \frac{1}{8.3 \cdot 10^5 \exp(-\frac{T_A}{T})}$  with  $T_A = 15100$  K.

#### 2.4 Manifold interpretation of the NE-EDC model

In the NE-EDC model, assumptions are made that lead to a representation of the mean reaction rate. However, the final result can be interpreted as a simplification similar to what is achieved by eliminating fast chemical degrees of freedom in a manifold method. The manifold interpretation is a way to describe how the NE-EDC model provides a description of the state properly taking into account the relative magnitude of both chemical and turbulent time scales. Following De et al. [19], it can be summarized as follows: According to the rate expression of Eq. (3), the local mean value of the mass fraction relaxes to a transient target value. Two time scales are involved: the target value is the value obtained by integrating the detailed kinetics over a time scale  $\tau^*$  given by  $\tau^* = C_\tau \left(\frac{\nu}{\varepsilon}\right)^{1/2} = C_\tau Re^{-1/2} \frac{k}{\varepsilon}$ . For  $C_\tau$  of order unity, this time scale is of the order of the Kolmogorov scale. The time scale controlling the relaxation rate is  $\tau_{mix}$ , given by  $\tau_{mix} = \frac{1-\xi^{*3}}{\xi^{*2}} \tau^* = (1-\xi^{*3}) \frac{C_\tau k}{C_\xi^2 \varepsilon}$ . For default values of the model coefficients, this parameter is of the order of the integral time scale. The model effectively projects the chemical evolution in such a manner that the chemical processes with a time scale shorter than the Kolmogorov scale are averaged out and only a subset of the composition space (a manifold) is reached. In the NE-EDC model, these time scales are dependent on the local Reynolds and Damköhler numbers. For example, in the NE-EDC model, the reacting time scale and mixing time scale can be defined as Eq. (24) and Eq. (25). Similar expressions can also be derived for the E-EDC model.

$$\tau^* = C_\tau \left(\frac{\nu}{\varepsilon}\right)^{1/2} = \frac{1}{2} \frac{1}{\sqrt{(Re_\tau + 1) Da^*}} \left(\frac{\nu}{\varepsilon}\right)^{1/2} \quad (24)$$

$$\tau_{mix} = (1 - \xi^{*3}) \frac{C_\tau k}{C_\xi^2 \varepsilon} = \frac{1}{3} (1 - \xi^{*3}) (Re_\tau + 1)^{-3/2} Da^{*-5/2} \frac{k}{\varepsilon} \quad (25)$$

### 3 Experimental and computational setup

The database used for model validation has been created by experimental measurements in the Delft lab-scale furnace performed by Huang [37]. The burner and the furnace are described in subsection 3.1, while the numerical setup is described in subsection 3.2.

### 3.1 Experimental furnace

The geometry of the Delft lab-scale furnace is shown in Figure 1. The furnace can operate in flameless mode thanks to the recuperative burner injecting fuel and preheated air in separate high momentum jets.

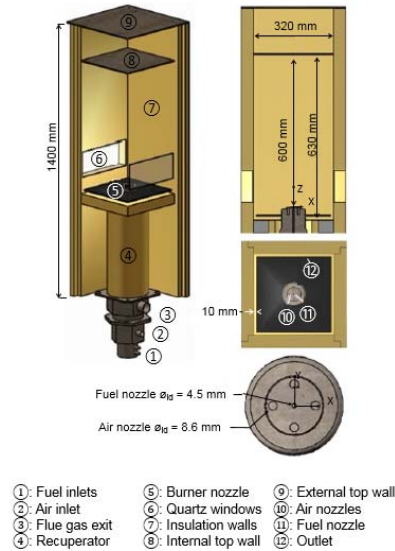


Figure 1. Delft Lab-scale furnace [37]

The internal dimensions of the furnace are 320 mm x 320 mm x 630 mm. The burner nozzle system is located at the bottom and consists of a central fuel nozzle ( $\varnothing_{id} = 4.5 \text{ mm}$ ) surrounded by four air nozzles ( $\varnothing_{id} = 8.6 \text{ mm}$ ). The nozzles protrude into the furnace by 30 mm, making the distance from the burner nozzle tip to the internal top wall equal to 600 mm. The flue gas outlet is a slit near the walls in the bottom plane, close to the burner (see point 12 of Figure 1). The start-up of the furnace is carried out using the injection of premixed fuel and air through the four outer nozzles. Once the furnace is preheated to 1123 K (850 °C), the burner is switched to injection for flameless mode with a non-premixed fuel and air combustion (fuel in the centre, air in the outer nozzles). The combustion gases leaving the furnace traverse a heat exchanger to preheat the air to a maximum temperature of 973 K (700 °C).

The experimental measurements, which are used to validate the modelling results, are obtained when the furnace operates with Dutch natural gas (mole fractions: CH<sub>4</sub> 81.3%, C<sub>2</sub>H<sub>6</sub> 3.7%, N<sub>2</sub> 14.4% and the rest 6%), which is injected into the furnace at 446 K, while the preheated air is injected at 886 K. The thermal input is 9 kW, with an equivalence ratio of 0.8 (see Table 3). The velocity and temperature measurements have been made, respectively, using Laser Doppler Anemometry (LDA) and Coherent Anti-stokes Raman Spectroscopy (CARS) (Table 2 provides information on the reported measurement accuracy). It should be mentioned that the furnace is optically accessible via small windows in the sidewall (see Figure 1), including one window used for LDA in backscatter mode and two windows for CARS. A Testo 335 flue gas analyser was used for product composition measurement, which has a resolution of 1 ppm for both CO and NO<sub>x</sub>, while the inaccuracy for the CO measurement is  $\pm 10 \text{ ppm}$  reading at 0-200 ppm for NO<sub>2</sub>. The flow

rates of fuel and air are measured using Bronkhorst mass flow controllers with an inaccuracy of  $\pm 0.5\%$  reading plus  $\pm 0.1\%$  full scale. Finally, super OMEGACLADTM XL sheathed ungrounded type K thermocouples were used for flue gas and wall temperature measurement.

Table 2 Technique and reported accuracy of the measured variables

Variable	Technique	Reported Accuracy
Velocity	LDA	2-8%
Temperature	CARS	20 K

To enable a fixed position of the optical equipment, the burner and top wall of the furnace are moved vertically to the appropriate position for taking measurements at a specific height above the nozzle exit. The top wall of the furnace acts as a heat sink. The sidewalls are well insulated, thus minimizing heat losses.

Table 3. Furnace operating conditions; thermal input power ( $P$ ), equivalence ratio ( $\phi$ ) and fuel and air flow rates ( $\dot{V}_f$  and  $\dot{V}_a$  respectively)

P (kW)	$\phi$	$\dot{V}_f$ (nl/min)	$\dot{V}_a$ (nl/min)
9	0.8	17.27	180.40

The measured experimental profiles do not have the mirror symmetry that would follow from the furnace design. This is attributed to the asymmetry in the fuel and air supply system upstream of the furnace [37]. To prepare for a fair comparison with the results of computations using perfectly symmetric inlets, all experimental mean profiles have been shifted in space in order to obtain close to symmetric results before comparison with the model results in Section 4. The measured profiles of mean velocity, turbulent kinetic energy and mean temperature data, from  $z=100$  to  $z=500$  mm, have been moved by a distance of  $z * \tan(\theta)$  before comparing them with the predictions. The value of the angle  $\theta$  is obtained considering that the shear stress has a value equal to zero on the centreline, and is  $\theta \approx 0.03$ .

### 3.2 Computational setup

The CFD code ANSYS Fluent, release 18.2 [40], has been used. A three-dimensional steady-state RANS modelling has been performed. Exploiting the furnace symmetry, a computational domain, covering only half of the furnace domain, is used. The domain starts upstream of the nozzle exit.

Figure 2 shows the computational grid used during the modelling, which was made using a blocking strategy. Thus, a structured non-uniform mesh, with hexahedral cells and O-grid in the centre of each nozzle exit, is used.



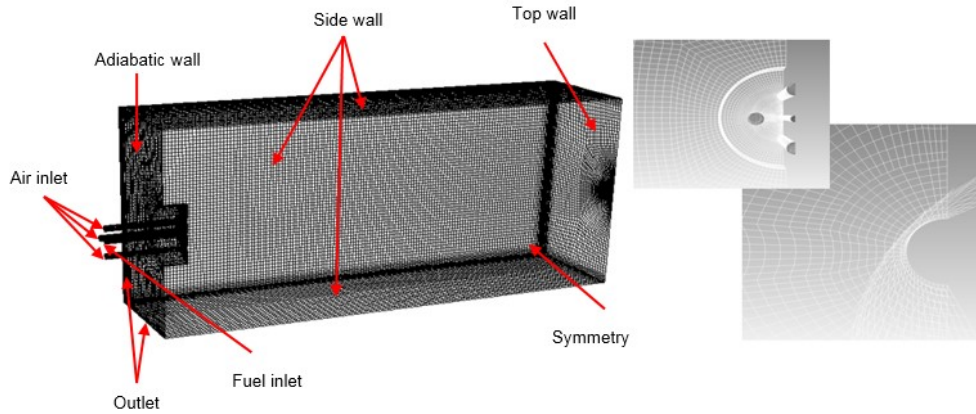


Figure 2. Three-dimensional view of the computational domain

Different turbulence-chemistry-interaction models are compared in this work, while keeping the other sub-models the same: the realizable two-equation  $k-\varepsilon$  turbulence model in combination with the Discrete Ordinates (DO) method, solving the radiative transfer equation using a grey weighted-sum-of-grey-gases model (WSGGM) for the absorption coefficient. The chemical mechanism is the DRM19 [49], having 19 species and 84 reactions.

Boundary conditions, however, are defined on the basis of the experimental setup (Figure 2). For example, the air and fuel inlet are defined as a mass flow type based on measured data, while the outlet is a pressure outlet boundary type. The thermal boundary conditions at the walls indicated in Figure 2 are: adiabatic on the bottom wall, a specified vertical temperature profile obtained through the interpolation of the measured data for the side walls and a constant temperature equal to the measured value for the top wall.

In order to ensure a good mesh quality, a grid sensitivity analysis was carried out using the Fluent EDC model with the default constant values of the model. The results from three different mesh sizes were compared: a precise mesh with 1.78 million elements; a medium size mesh with 800,000 cells; and a coarse mesh with 350,000 elements. The Grid Convergence Index ( $GCI_{\text{coarse}}$ ) method (based on the Richardson extrapolation method) was chosen to quantify the discretization error [50]-[51]. In the case under study, the  $GCI_{\text{coarse}}$  value was 3.1% for turbulence kinetic energy at the furnace outlet, using the base grid with about 800,000 cells (lower than the maximum recommended, which is 5%). Therefore, this was the selected grid size to carry out further modelling. It can be stated that the grid provides accuracy and consistency in the results on the one hand, and an acceptable CPU time on the other (run time for a 4 cores CPU@ 2.5 GHz is around 2 days, with a convergence level below  $1e-5$  for turbulence kinetic energy).

Finally, for the implementation of the E-EDC and NE-EDC models, the reaction rates have been specified with User Defined Functions.

## 4 Results of flameless combustion modelling

This section presents the modelling results. First, an appropriate  $C_\xi$  is determined for use in the EDC model with constant model parameters. Then, the NE-EDC model mean temperature profiles are compared with the E-EDC model results. Finally, the predictions of velocity and temperature fields in three models (the NE-EDC model, the EDC model with specific and optimized fixed values of the model constants, and the Flamelet Generated Manifold (FGM) model, which is based on pure fuel and air as boundary conditions for flamelet generation) are presented and compared with experimental data.

### 4.1 $C_\xi$ model constant value selection

To determine an appropriate  $C_\xi$  value for applying the EDC model to a flameless combustion furnace, the position of the zone with a high heat release, as known from the  $\text{OH}^*$  measurements, is used as the criterion. Thus, the degree of spatial homogeneity of the mean temperature, as known from the CARS measurements, is predicted correctly. As a numerical parameter representing the reaction zone, the product of the formaldehyde ( $\text{CH}_2\text{O}$ ) mass fraction and the  $\text{OH}$  mass fraction [52]-[53], called formylradical (HR), is used. The mass fraction of  $\text{CH}_2\text{O}$  indicates when the reaction starts, while the latter indicates that a high temperature has been reached. Figure 5 shows the contour plot of the formylradical for six values of the parameter  $C_\xi$ , from the standard value to higher values.

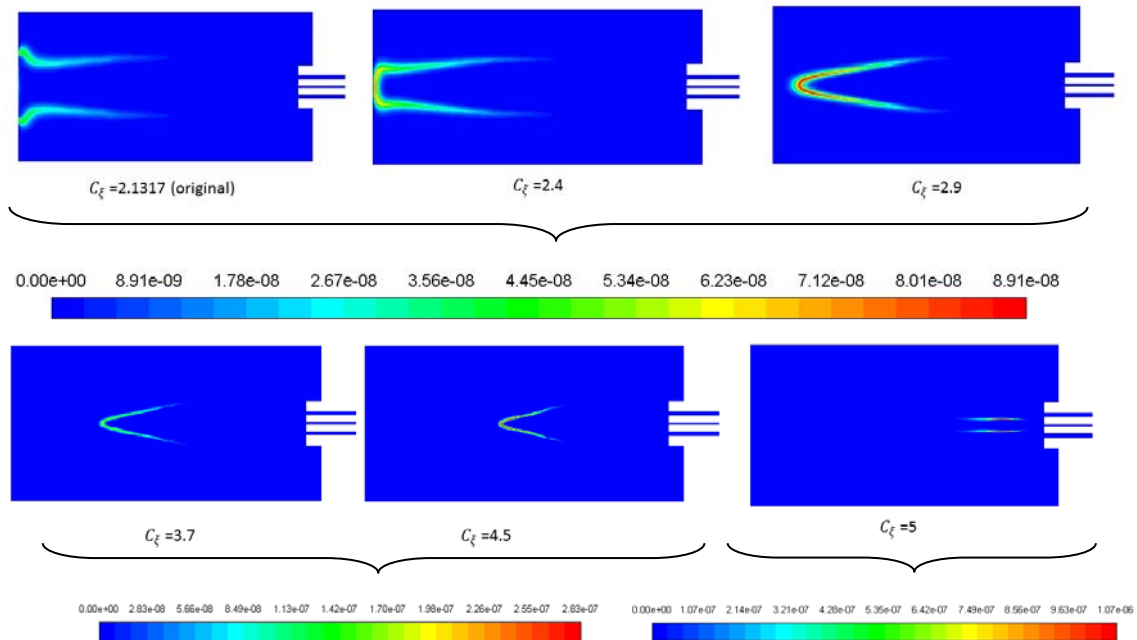


Figure 3 Predicted formylradical (HR) for different  $C_\xi$  values

According to the mean  $\text{OH}^*$  chemiluminescence intensity distribution, reported by Huang [37] for an equivalence ratio of 0.8, the reaction zone is located in the middle of the furnace between 450 mm and 550 mm above the burner nozzle. This is incompatible with the predictions for  $C_\xi=2.1317$ ,

2.4 and 5. For the values  $C_\xi=2.1317$  and 2.4, the reaction zone is too high, while for  $C_\xi=5$  it is too low. For the choice between the other values, the homogeneity of the mean temperature (see Figure 4) is used as the quality measure.

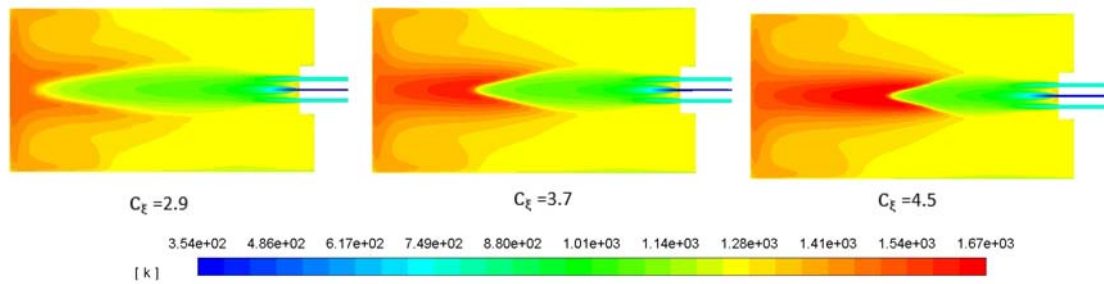


Figure 4 Temperature contour for several  $C_\xi$  values

The best temperature homogeneity is found for  $C_\xi=2.9$ ; however, further analysis and a more detailed comparison with experimental data of velocity and temperature are necessary (see subsections 4.3 and 4.4).

#### 4.2 Comparison of E-EDC and NE-EDC

The relative performance of the E-EDC and the NE-EDC models is validated by looking at the prediction of mean velocity and temperature. For the velocity fields, the differences are very small. For the temperature, noticeable differences show up only in the upper part of the furnace, at  $z=300$  mm and higher. The experimental measurements and the results of the two models are shown in Figure 5.

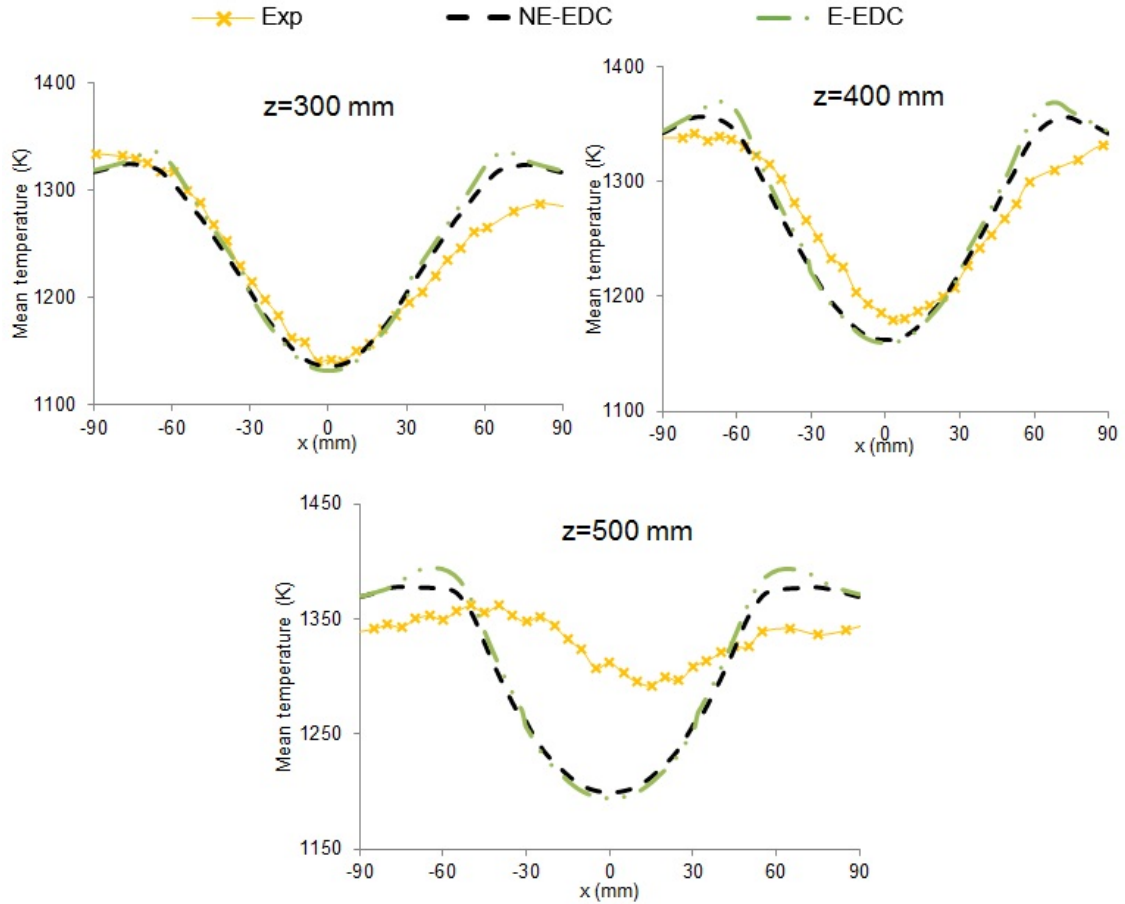


Figure 5 Comparison between E-EDC and NE-EDC mean temperature

The temperature prediction close to the centre ( $x=0$  mm) is essentially the same in both models. However, away from the centre ( $|x| > 60$  mm), the temperature is less over predicted by the NE-EDC model for the three heights. Therefore, the NE-EDC gives a better prediction of the radial profiles of the mean temperature as compared to the E-EDC. For this reason, in the next sections, the E-EDC is left out of consideration.

#### 4.3 Comparison of EDC, NE-EDC, and FGM: velocity field

In Figure 6, the radial profiles of the mean axial velocity ( $\tilde{U}_z$ ) at different axial locations, predicted by the three considered models, are compared with the experimental data (the EDC model with modified  $C_\xi$  constant value is called the EDC mod in the figures). The mean velocity  $\tilde{U}_z$  at the nozzle exit, by construction, agrees well with the experimental data, but as the flows develop ( $z=50$  mm), the peak velocity on the centreline of the air jets is over predicted.

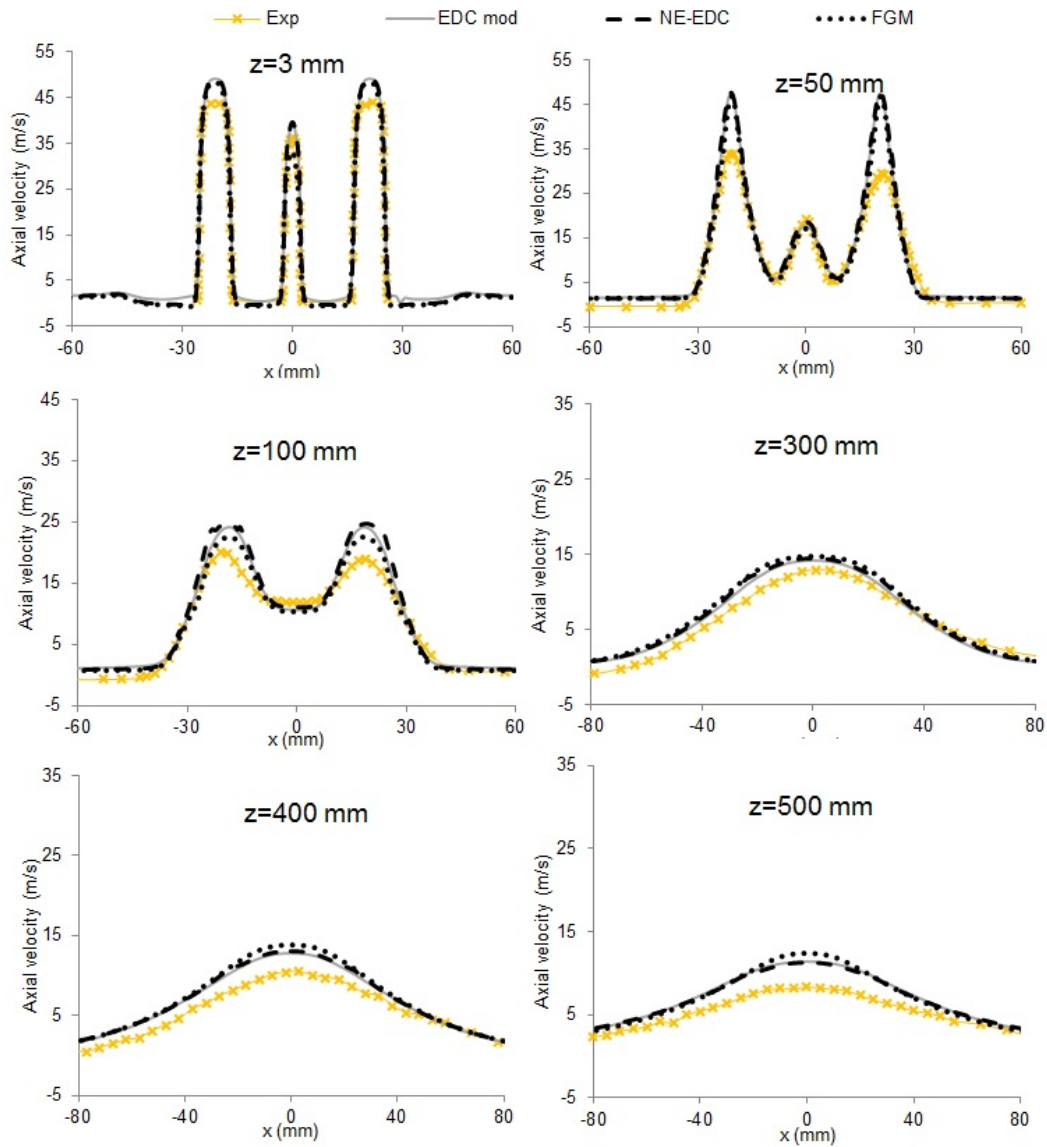


Figure 6 Comparison between measured and predicted radial profiles of mean axial velocity.

At the mid-height of the furnace ( $z=100$  and  $z=300$  mm), the three model results are in good agreement with the experimental data, showing an acceptable performance of the realizable  $k - \varepsilon$  model. At larger heights ( $z=400$  and  $500$  mm), the predicted axial velocity is also in good agreement with the experimental data. However, the FGM model slightly over predicts the mean axial velocity. This can be attributed to the fact that the FGM model over predicts the mean temperature (see subsection 4.4); hence, following the laws of momentum conservation, under predicting the density leads to an over prediction of the velocity.

Next, the mean turbulent kinetic energy predicted by the  $k - \varepsilon$  model is analysed. Representative radial profiles are shown in Figure 7. At the inlet, the boundary condition for turbulent kinetic energy is derived from the measured data for the axial and radial directions and then multiplying the contribution of the radial direction by two to account for the contribution from the non-measured direction. At  $z=100$  mm, the three models over predict the mean turbulent kinetic energy. The EDC models are over predicting the mean turbulent kinetic energy more than the

FGM, in spite of the fact that they were slightly more accurate predicting the mean axial velocity (Figure 6). At  $z=500$  mm, the predictions are quantitatively better, but the minimum at the centreline shows that the rate of jet development is under predicted.

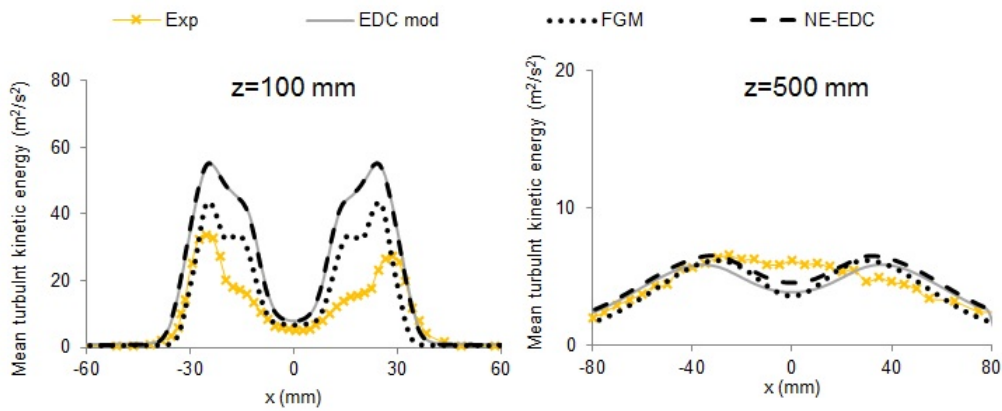


Figure 7 Comparison between measured and predicted mean turbulence kinetic energy

#### 4.4 Comparison of EDC, NE-EDC, and FGM: mean temperature field

Next, a comparison is made between the measured and predicted mean temperatures obtained for each turbulence-chemistry model. In Figure 8, the mean temperature contour plots are shown for each of the studied turbulence-chemistry interaction models.

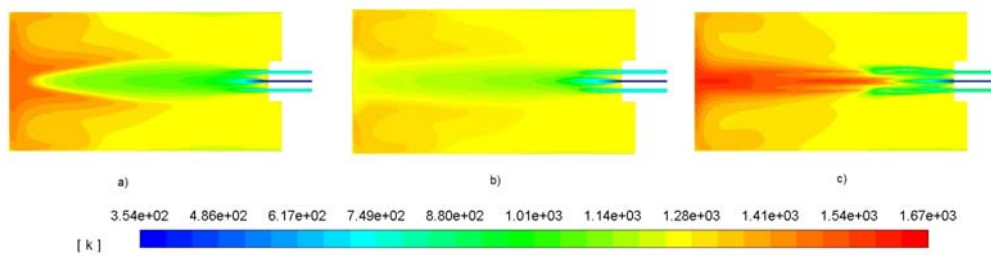


Figure 8 Temperature contour a) EDC Model Constant  $C_{\xi} = 2.9$ , b) NE-EDC and c) FGM Model

The EDC model with global change of model constant,  $C_{\xi}$ , equal to 2.9 (Figure 8a)), predicts a quite homogeneous temperature in the area close to the burner (up to  $z=200$  mm); however, in the top zone of the furnace ( $500 \text{ mm} < z < 400 \text{ mm}$ ), a maximum temperature of around 1450K is predicted.

In the NE-EDC model (Figure 8b), where  $C_{\tau}$  and  $C_{\xi}$  are space dependent, since they are calculated directly on the basis of the local Reynolds number and the Kolmogorov scale Damköhler number, the predicted temperature distribution is very homogeneous along the entire height of the furnace.

Finally, the FGM model (Figure 8c) predicts a non-uniform temperature distribution showing a high temperature zone in the middle of the furnace.

A quantitative comparison with experimental data can be made by looking at the mean temperature profiles along horizontal cross sections at different heights above the nozzle exit, shown in Figure 9. It can be clearly seen that the FGM does not perform as well as the EDC, with the NE-EDC providing the best prediction of all.

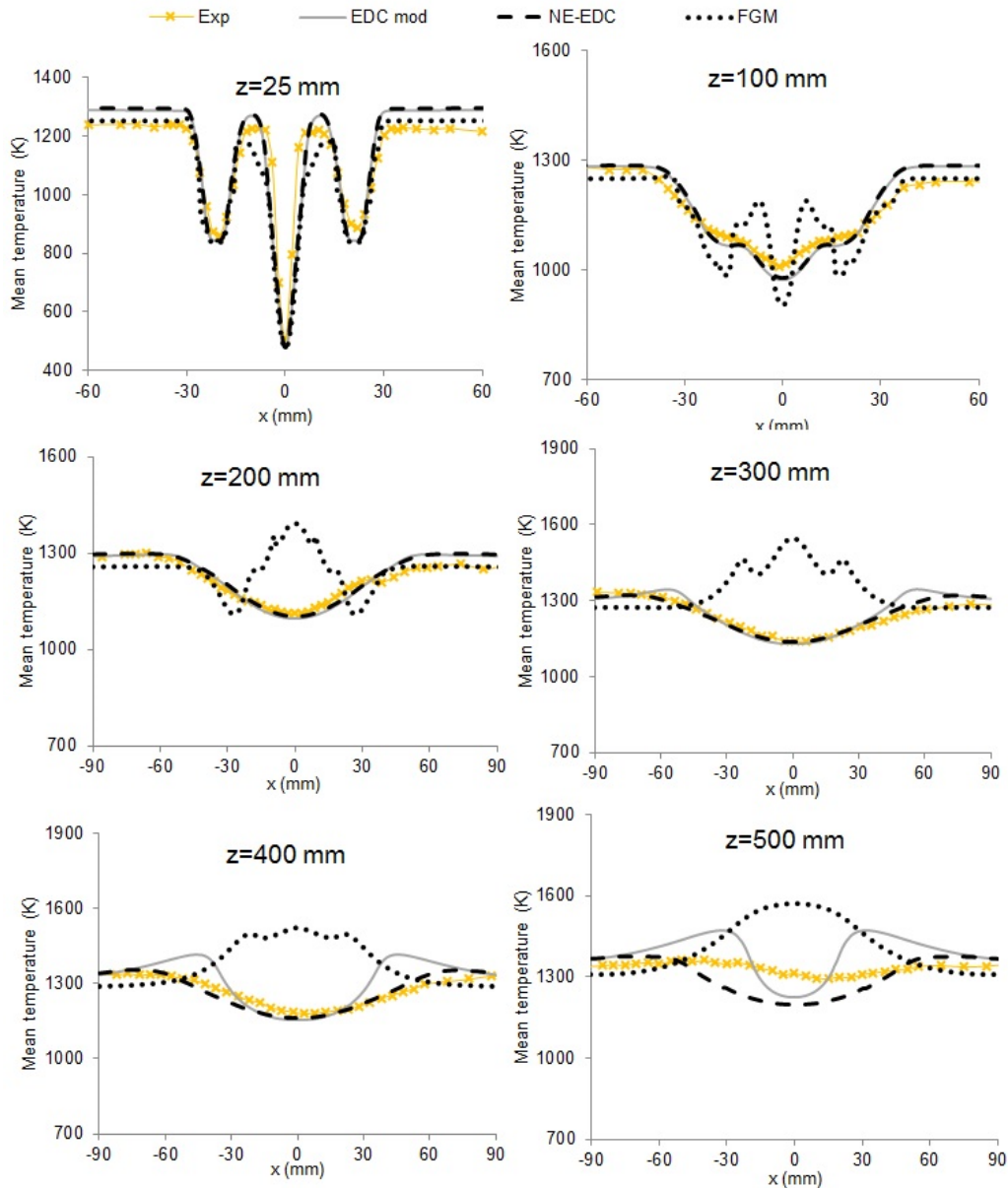


Figure 9. Comparison of mean temperature from experimental measurements and from simulations with EDC model with  $C_{\xi} = 2.9$ , NE-EDC model and FGM model

The FGM model over predicts the mean temperature significantly along almost the entire height of the furnace. In fact, as the distance from the centre increases, the gradient becomes the opposite to that of the experimental data. The simulation results and experimental data are only quite close at  $z=25$  mm. Although fuel and air are injected at a distance from each other, the FGM, based on counterflow non-premixed flamelets of fuel and air, including the PDF model for the

fluctuations of mixture fraction and progress variable, performs well in the region close to the burner. Further downstream, however, where the dilution is dominant, the model fails.

The EDC model, with  $C_\xi = 2.9$ , provides predictions for mean temperatures that are in close agreement with the experimental results in the area close to the burner ( $z=25$  mm,  $z=100$  mm and  $z=200$  mm). However, at  $z=300$  mm, a deviating trend appears that shows a local maximum away from the centre. At  $z=400$  mm, this deviation is larger in magnitude, but still restricted to the zone far from the centre. In the top zone of the furnace ( $z=500$  mm), there is also an under prediction in the central region. In short, the EDC model, with a finite structure constant value equal to 2.9, does not predict the mean temperature profile in the upper part of the furnace very accurately.

The NE-EDC model, in the lower part of the furnace ( $z=25$  mm,  $z=100$  mm,  $z=200$  mm), gives a temperature prediction that is as good as that of the EDC model with  $C_\xi = 2.9$ . However, in the middle ( $z=300$  mm) and upper ( $z=400$  mm) zones of the furnace, the results are in better agreement with the experimental data; in fact, better than the EDC model with a globally modified  $C_\xi$ . At  $z=300$  and  $z=400$  mm, the temperature over prediction far from the centre is smaller for the NE-EDC. At  $z=500$  mm, the temperature is under predicted in the centre. So it can be concluded that the NE-EDC model is a real improvement in comparison to the EDC model with constant  $C_\xi$ . Referring back to the comparison between the E-EDC and the NE-EDC in Figure 5, the NE-EDC brings a slight improvement in the middle and upper zones of the furnace.

## 5 Conclusions

In this work, the NE-EDC was derived and its performance validated in comparison with the EDC with constant calibrated model constant, the E-EDC model developed by Parente and the FGM model based on non-premixed flamelets of fuel and air. Detailed experimental data available from previous work on a natural gas fired lab-scale furnace were used. The E-EDC and the NE-EDC models differ from the standard EDC model implemented in ANSYS Fluent by the fact that the two key model constants are dependent on the local Reynolds number and the Kolmogorov scale Damköhler number. The first difference between these two extended models is in the different assumptions concerning the fine structure length scale (NE-EDC assumes  $L^* = \eta_k$ , while E-EDC has  $L^* \neq \eta_k$ ). The second is the different representation of the laminar flame speed. The NE-EDC model proposes a laminar flame speed definition based directly on the length and time scales.

It is found that the FGM model described the near burner zone dominated by separate jets of fuel and air quite well, but fails to capture the flameless mode further downstream in the furnace. The predicted mean temperature gradients show erroneous trends and the mean temperature is over predicted. The root cause of this appears to be the use of undiluted flamelets. In an earlier calculation of this furnace, where diluted flamelets were used, the FGM showed a better agreement [37]. The fact that flamelet based models, based on diluted flamelets, perform better than standard undiluted flamelets in flameless combustion is in agreement with the analysis of



DNS simulation results presented in Ref. [31]. The ANSYS Fluent default FGM option does not allow for the dilution of the flamelets and could not be used in this study.

The EDC model with finite constant value, set at  $C_{\xi} = 2.9$ , provides better results than the FGM model, but they are not as good as the E-EDC and the NE-EDC. The E-EDC and the NE-EDC models offer a significant advantage over the EDC model with globally modified  $C_{\xi}$  value. In the latter (the EDC model), there is a need for a parametric calibration in order to optimize the  $C_{\xi}$  value for the case study and this is not needed in the other two because the  $C_{\xi}$  is evaluated on the basis of the local Re and Da numbers. The NE-EDC modelling results and experimental profiles match very well at all heights, even though the mean temperature is a little under predicted at the highest analysed height ( $z=500$  mm). Using more information from a detailed mechanism to obtain an appropriate chemical time scale, as proposed by Evans et al. [35], could be a means to improve this aspect.

The velocity and turbulence predictions of the NE-EDC and the E-EDC models are very close to each other; while the mean temperature results in the lower part of the furnace are also very close. Differences only appear in the upper part of the furnace. Here, the NE-EDC gives a more accurate prediction of the radial profiles of the mean temperature, especially far from the centre. This demonstrates that the differences between the E-EDC and the NE-EDC model assumptions lead to a different  $C_{\xi}$  formulation (see Eq. (19) and Eq. (23)), and finally, a different mean reaction rate is also relevant.

## References

- [1] J. A. Wüning, J. G. Wüning, Flameless oxidation to reduce thermal NO-formation, *Prog. Energy Combust. Sci.* 23 (1997) 81-94.
- [2] A. Cavaliere, M. de Joannon, M. Mild combustion, *Prog. Energy Combust. Sci.* 30 (2004) 329-366.
- [3] N. Romero-Anton, K. Martin-Eskudero, L.A. Portillo-Valdes, I. Gomez-Elvira, E. Salazar-Herran, E. Improvement of auxiliary BI-DRUM boiler operation by dynamic simulation. *Energy* 148 (2018) 676-686.
- [4] A.A.V. Perpignan, A. Gangoli-Rao, D.J.E.M. Roekaerts, Flameless combustion and its potential towards gas turbines, *Prog. Energy Combust. Sci.* 69 (2018) 28-62.
- [5] B.B. Dally, A.N. Karpetis, R.S. Barlow, Structured of turbulent non-premixed jet flames in a diluted hot flow, *Combust. Flame* 27 (2002) 2255-2265.
- [6] R. Cabra, T. Myhrvold, J.Y. Chen, R.W. Dibble, A.N. Karpetis, R.S. Barlow, Simultaneous laser raman-rayleigh-lif measurements and numerical modeling results of a lifted turbulent  $H_2/N_2$  jet flame in a vitiated coflow, *Proc. Combust. Inst.* 29 (2002) 1881-1888.
- [7] E. Oldenhof, M.J. Tummers, E.H. van-Veen, D.J. E.M. Roekaerts, Conditional flow field statistics of jet-in-hot-coflow flames, *Combust. Flame* 160 (2013) 1428-1440.
- [8] C. Duwig, B. Li, Z.S. Li, M. Aldén, High resolution imaging of flameless and distributed turbulent combustion, *Combust. Flame* 159 (2012) 306-316.

- [9] T. Plessing, N. Peters, J.G. Wüning, Laser optical investigation of highly preheated combustion with strong exhaust gas recirculation, *Symp. (Int.) Combust.* 27 (1998) 3197-3204.
- [10] A. Cavigiolo, M.A. Galbiati, A. Effuggi, D. Gelosa, R. Rota, Mild combustion in a laboratory-scale apparatus, *Combust. Sci. Technol.* 175 (2003) 1347-1367.
- [11] A.S. Verissimo, A.M.A. Rocha, M. Costa, Operational, Combustion and Emission Characteristics of a Small-Scale Combustor, *Energy Fuels* 25 (2011) 2469-2480.
- [12] A. Rebola, M. Costa, P.J. Coelho, Experimental evaluation of the performance of a flameless combustor, *Appl. Therm. Eng.* 50 (2013) 805-815.
- [13] G. Sorrentino, P. Sabia, M. de-Joannon, R. Ragucci, A. Cavaliere, U. Göktolga, J. van-Oijen, P. de-Goey, Development of a Novel Cyclonic Flow Combustion Chamber for Achieving MILD/Flameless Combustion, *Energy Procedia* 66 (2015) 141-144.
- [14] C. Galletti, A. Parente, L. Tognotti, Numerical and experimental investigation of a mild combustion burner, *Combust. Flame* 151 (2007) 649-664.
- [15] A. Parente, C. Galletti, L. Tognotti, Effect of the combustion model and kinetic mechanism on the MILD combustion in an industrial burner fed with hydrogen enriched fuels, *Int. J. Hydrogen Energy* 33 (2008) 7553-7564.
- [16] B. Danon, E.S. Cho, W. de-Jong, D.J.E.M. Roekaerts, Parametric optimization study of a multi-burner flameless combustion furnace, *Appl. Therm. Eng.* 31 (2011) 3885-2896.
- [17] D. Tabacco, C. Innarella, C. Bruno, Theoretical and Numerical Investigation on Flameless Combustion, *Combust. Sci. Technol.* 174 (2002) 1-35.
- [18] F.C. Christo, B.B. Dally, Modeling turbulent reacting jets issuing into a hot and diluted coflow, *Combust. Flame* 142 (2005) 117-129.
- [19] A. De, E. Oldenhof, P. Sathiah, D.J.E.M. Roekaerts, Numerical Simulation of Delft-Jet-in-Hot-Coflow (DJHC) Flames Using the Eddy Dissipation Concept Model for Turbulence–Chemistry Interaction, *Flow Turbul. Combust.* 87 (2011) 537-567.
- [20] J. Aminian, C. Galletti, S. Shahhosseini, L. Tognotti, Numerical Investigation of a MILD Combustion Burner: Analysis of Mixing Field, Chemical Kinetics and Turbulence-Chemistry Interaction, *Flow Turbul. Combust.* 88 (2012) 597-623.
- [21] M. Rehm, P. Seifert, B. Meyer, Theoretical and numerical investigation on the EDC-model for turbulence–chemistry interaction at gasification conditions, *Comput. Chem. Eng.* 33 (2009) 402-407.
- [22] A. Mardani, Optimization of the Eddy Dissipation Concept (EDC) model for turbulence-chemistry interactions under hot diluted combustion of CH<sub>4</sub>/H<sub>2</sub>, *Fuel* 191 (2017) 114-129.
- [23] M.T. Lewandowski, I.S. Ertesvåg, Analysis of the Eddy Dissipation Concept formulation for MILD combustion modelling, *Fuel* 224 (2018) 687-700.
- [24] I.S. Ertesvåg, Analysis of Some Recently Proposed Modifications to the Eddy Dissipation Concept (EDC), *Combust. Sci. Technol.* (2019) 1-29.
- [25] B.F. Magnussen, B. Hjertager, On the structure of turbulence and a generalized eddy dissipation concept for chemical reaction in turbulent flow, 19<sup>th</sup> AIAA Aerospace Meeting, St. Louis (1981).
- [26] B.F. Magnussen, The eddy dissipation concept a bridge between science and technology. ECCOMAS thematic conference on computational combustion, Lisbon, Portugal (2005).

- [27] A. Parente, M.R. Malik, F. Contino, A. Cuoci, B.B. Dally, Extension of the Eddy Dissipation Concept for turbulence/chemistry interactions to MILD combustion, *Fuel* 163 (2016) 98-111.
- [28] Z. Chen, V. M. Reddy, S. Ruan, N. A. K. Doan, W. L. Roberts, N. Swaminathan, Simulation of MILD combustion using Perfectly Stirred Reactor model, *Proc. Combust. Inst.* 36 (2017) 4279-4286.
- [29] Z. X. Chen, N. A. K. Doan, X. J. Lv, N. Swaminathan, G. Ceriello, G. Sorrentino, A. Cavaliere, Numerical study of a cyclonic combustor under moderate or intense low-oxygen dilution conditions using non-adiabatic tabulated chemistry. *Energy Fuels* 32 (2018) 10256-10265.
- [30] Y. Minamoto, T. D. Dunstan, N. Swaminathan, R. S. Cant, DNS of EGR-type turbulent flame in MILD condition, *Proc. Combust. Inst.* 34 (2013) 3231-3238.
- [31] Y. Minamoto, N. Swaminathan, N. Modelling paradigms for MILD combustion, *Int J Adv Eng Sci Appl Math.* 6 (2014) 65-75.
- [32] Y. Minamoto, N. Swaminathan, Scalar gradient behaviour in MILD combustion, *Combust. Flame* 161 (2014) 1063-1075.
- [33] Y. Minamoto, N. Swaminathan, R. S. Cant, T. Leung, Reaction zones and their structure in MILD combustion, *Combust. Sci. Technol* 186 (2014) 1075-1096.
- [34] B. B. Dally, E. Riesmeier, N. Peters, Effect of fuel mixture on moderate and intense low oxygen dilution combustion, *Combust. Flame* 137 (2004) 418-431.
- [35] M. J. Evans, C. Petre, P. R. Medwell, A. Parente, Generalisation of the eddy-dissipation concept for jet flames with low turbulence and low Damköhler number, *Proc. Combust. Inst.* 37 (2019) 4497-4505.
- [36] X. Huang, M.J. Tummers, D.J.E.M. Roekaerts, Experimental and numerical study of MILD combustion in a lab-scale furnace, *Energy Procedia* 120 (2017) 395-402.
- [37] X. Huang, Measurements and Model Development for Flameless Combustion in a lab-scale furnace, Ph. D. Thesis, Delft University of Technology (2018).
- [38] F.C. Christo, B. Dally, Application of transport PDF approach for modelling MILD combustion, 15<sup>th</sup> Australasian Fluid Mechanics Conference (2004).
- [39] D. Lupant, P. Lybaert, Assessment of the EDC combustion model in MILD conditions with in-furnace experimental data, *Appl. Therm. Eng.* 75 (2015) 93-102.
- [40] Fluent Manual. Ansys Fluent Theory guide 18.2. ANSYS Inc, Canonsburg, PA (2017).
- [41] I.R. Gran, B.F. Magnussen, A Numerical Study of a Bluff-Body Stabilized Diffusion Flame. Part 2. Influence of Combustion Modeling And Finite-Rate Chemistry, *Combustion Sci. Technol.* 119 (1996) 191-217.
- [42] P. Glarborg, R.J. Kee, J.F. Gracar, J.A. Miller, PSR: A Fortran Program for Modeling Well-Stirred Reactors. Sandia National Labs, Livermore, CA (USA); Report (1986) 8186-8209.
- [43] Z. Li, A. Cuoci, A. Sadiki, A. Parente, Comprehensive numerical study of the Adelaide Jet in Hot-Coflow burner by means of RANS and detailed chemistry, *Energy* 139 (2017) 555-570.
- [44] I.S. Ertesvåg, B.F. Magnussen, The Eddy Dissipation Turbulence Energy Cascade Model, *Combust. Sci. Technol.* 159 (2000) 213-235.
- [45] M. Graça, A. Duarte, P.J. Coelho, M. Costa, Numerical simulation of a reversed flow small-scale combustor, *Fuel Proc. Technol.* 107 (2013) 126-137.
- [46] T. Poinso, D. Veynante, Theoretical and numerical combustion, RT Edwards (2005).

- [47] K. K. Kuo, R. Acharya, Fundamentals of turbulent and multiphase combustion, John Wiley & Sons (2012).
- [48] E. Oldenhof, M. J. Tummers, E. H. Van Veen, D. J. E. M. Roekaerts, Ignition kernel formation and lift-off behaviour of jet-in-hot-coflow flames, Combust. Flame 157 (2010) 1167-1178.
- [49] A. Kazakov, M. Frenklach, GRI-Mech 1.2, <http://combustion.berkeley.edu/drm/>. (Accessed October 2018).
- [50] I. Celik, U. Ghia, P.J. Roache, C. Freitas, H. Coloman, P. Raad, Procedure of Estimation and Reporting of Uncertainty Due to Discretization in CFD Applications, J. Fluids Eng. 130 (2008) 078001
- [51] P.J. Roache, Quantification of uncertainty in computational fluid dynamics, Annu. Rev. Fluid Mech. 29 (1997) 123-160.
- [52] P.R. Medwell, P.A.M. Kalt, B.B. Dally. Simultaneous imaging of OH, formaldehyde, and temperature of turbulent nonpremixed jet flames in a heated and diluted coflow, Combust. Flame 148 (2007) 48-61.
- [53] R.L. Gordon, A.R. Masri, E. Mastorakos, Simultaneous Rayleigh temperature, OH-and CH<sub>2</sub>O-LIF imaging of methane jets in a vitiated coflow, Combust. Flame 155 (2008) 181-195.